

CO(J=2-1) Observations of the Circumstellar Envelope of Betelgeuse with CARMA

Eamon O'Gorman and Graham M. Harper

School of Physics, Trinity College Dublin, Dublin 2, Ireland

`eogorma@tcd.ie`

`graham.harper@tcd.ie`

Joanna M. Brown

Harvard-Smithsonian Center for Astrophysics, 60 Garden Street,
MS-78, Cambridge, MA 02138, USA

`jbrown@mpe.mpg.de`

and

Alexander Brown

Center for Astrophysics and Space Astronomy, University of Colorado,
389 UCB, Boulder, CO 80309, USA

`alexander.brown@colorado.edu`

Received _____; accepted _____

ABSTRACT

We report the first radio interferometric observations of the 1.3 mm emission line of $^{12}\text{C}^{16}\text{O}$ in the circumstellar envelope of the M supergiant α Ori. Observations are made with the CARMA interferometer in the C, D, and E antenna configurations. We obtain excellent uv-coverage (6 - 27 $k\lambda$) by combining data from all three configurations allowing us to trace spatial scales from $0.8''$ to $4''$. The high spatial resolution C configuration map shows that the inner S1 shell has asymmetric outflow velocities of -10 km s^{-1} and $+13 \text{ km s}^{-1}$ with respect to the stellar rest frame. We find no evidence for the outer S2 shell in this configuration and assume that this emission has been resolved out. The S2 shell appears as an extra blueshifted emission component in the D and E configuration maps between -10 km s^{-1} and -16 km s^{-1} but we see no trace of it in the redshifted velocity component and we conclude that the S2 shell is asymmetric in velocity space. A discrete off-source emission feature is detected at $5''$ S-W of α Ori in all D configuration maps. We image both shells in the combined map (all configurations) revealing their complex and irregular structure. We assign an average outer radius of $5''$ to S1 and believe that S2 may extend beyond our field of view of $32''$.

Subject headings: circumstellar matter — Stars: individual: (α Ori) — Stars: late-type — Stars: massive — supergiants — Radio lines: stars

1. Introduction

Graham?

2. Observations and Data Reduction

The data were acquired with the 15 element CARMA (Combined Array for Research in Millimeter-wave Astronomy) (Scott et al. 2004) interferometer which is located at Cedar Flat in eastern California and consists of nine 6.1 m antennas and six 10.4 m antennas. Table 1 summarizes our various tracks of millimeter observations which span the period 2007 May - 2009 November. The observations consist of on source profiles of the $^{12}\text{C}^{16}\text{O}$ ($J=2-1$) line in the C, D and E array configurations. The baseline length spans over 30-350 m (C array), 11-150 m (D array) and 8-66 m (E array) providing spatial resolutions of 0.8'', 1.8'' and 4'' respectively at 1.3 mm.

The receivers were tuned to the $^{12}\text{C}^{16}\text{O}$ ($J=2-1$) line which has a rest frequency of 230.53 GHz (1.3 mm). The CARMA correlator takes measurements in three separate bands, each having an upper and lower sideband. One band was set to the low resolution 468 MHz (with 15 channels) mode to observe continuum emission and was centered on the line. The other two bands were configured with 62 MHz and 31 MHz bandwidth across 63 channels (with a resolution of 1.3 km s^{-1} and 0.65 km s^{-1} respectively) and were also centered on the line. The line was measured in the upper sideband in the C and E array and in the lower sideband in the D array.

Bandpass and phase calibration were performed using 3C120 and 0530+135. 0532+075 was used as a secondary phase calibrator to determine the quality of the phase transfer from the primary phase calibrator. The observing sequence was to integrate on the primary phase calibrator for ~ 2.5 minutes, the target for ~ 18 minutes, and the secondary phase

calibrator for ~ 2.5 minutes. The cycle was repeated for each track which lasted between 1.5 hours and 5 hours. Absolute flux calibration was carried out using the bandpass and phase calibrators in the continuously updated CARMA flux catalog.

The raw data was initially Hanning smoothed within MIRIAD¹ and then exported into FITS format so that it could be analyzed with the CASA² data reduction package. All calibration and imaging was carried out within CASA. The image cubes were multi-scale CLEANed down to the 3σ threshold using natural weighting and were corrected for primary beam attenuation, unless otherwise stated below. The *multiscale* algorithm (Rich et al. 2008) within CASA was set to four unique scales; the largest corresponding to the the largest structures visible in individual channel maps. Each scale was approximately set to three times larger than the preceding scale.

3. Results

3.1. Individual Configuration Image Cubes

The spectrum for each individual configuration image cube (which are composed of all the individual configuration tracks listed in Table 1) can be used to obtain information on the kinematics of both shells. The three corresponding spectra are shown in Figure 1 for both the high (0.65 km s^{-1}) and low (1.3 km s^{-1}) resolution data and were obtained by extracting all emission within a circular area centered on the source. The radii for these circular areas were $1''$, $4''$ and $8''$ for the C, D and E array image cubes respectively. The velocity rest frames of the spectra are plotted with respect to the stellar rest frame using a

¹Multichannel Image Reconstruction, Image Analysis and Display,
<http://www.atnf.csiro.au/computing/software/miriad/>

²Common Astronomy Software Applications, <http://casa.nrao.edu/>

radial velocity of 20.7 km s^{-1} derived by Harper et al. (2008).

The spectrum from the C array image cube has a total line width of 23 km s^{-1} and is dominated by three features; a blue wing, a red wing and a central emission feature at $\sim 0 \text{ km s}^{-1}$. The blue wing of the CO emission profile extends to -10 km s^{-1} while the red wing extends to $+13 \text{ km s}^{-1}$. The spectra from the D and E array image cubes have an additional blue wing emission feature located between -10 km s^{-1} and -16 km s^{-1} . This emission features appears to have been resolved out by the extended C antenna array which has a maximum scale of $\sim 4.5''$ but is detected by the more compact configurations which are more sensitive to extended emission. The total line width of the D and E array spectra are both 29 km s^{-1} . In all three spectra the high and low resolution data match verifying the existence of the main emission features in these line profiles.

An additional spatially unresolved source is detected in the D configuration image cube and has been previously documented by Harper et al. (2009). The component is present between $\sim -5 \text{ km s}^{-1}$ and $+6 \text{ km s}^{-1}$ and is located $\sim 5''$ S-W of α Ori. Its peak emission lies at $\sim 0 \text{ km s}^{-1}$ and is approximately equal to 60% of the source peak emission. The corresponding channel maps in the E configuration image cube show extended emission out to $8''$ in the same S-W direction as shown in Figure 2, but the source does not appear to be separate from α Ori. Curiously this second source does not appear in any of the C configuration image cube channel maps.

3.2. Multi-Configuration Image Cube

Figure 3 shows a subset of channel maps from the combined image cube. The first two channel maps show the continuum emission with no extended features apparent. Between -16.7 km s^{-1} and -10.3 km s^{-1} we see evidence for the development of a classical shell

signature. We first sample the highest velocity shell components where the emission is relatively compact (i.e. between -16.7 km s^{-1} and -12.9 km s^{-1}) and then sample lower velocity components where the shell becomes a faint ring (i.e. between -11.6 km s^{-1} and -10.3 km s^{-1}). These rings then either disappear into the noise of the channel maps or out of our field of view. Remarkable, this shell like structure is not seen in the corresponding red-shifted channel maps. All other channel maps out to a velocity of $+13 \text{ km s}^{-1}$ show some form of compact emission as can be seen in the final two channel maps between -9 km s^{-1} and -7.8 km s^{-1} . This emission extends out to an average distance of $\sim 5''$ but it is difficult to see evidence for shell development.

The spectra in Figure 4 are taken from the combined image cube using circular extraction areas ranging in radius from $1''$ to $10''$. All spectra have a total linewidth of 29 km s^{-1} which is in close agreement with previous single dish observations of the line (Knapp et al. 1980; Huggins 1986; Huggins et al. 1994). The most striking feature of these spectra is the change in appearance of the blueshifted emission component located between -16 km s^{-1} and -10 km s^{-1} . At small extraction radii, where we sample the compact emission, this emission feature is weak in comparison to the rest of the line. However, as we take larger extraction radii, we begin to sample more and more of the extended emission and this emission feature gets stronger until it eventually becomes the dominant component of the line.

4. Discussion and Conclusions

The two distinct velocity components seen by Bernat et al. (1979) in CO absorption against the stellar spectrum at $4.6 \mu\text{m}$ have both been detected at 230 GHz for the first time. The first velocity component known as S1 has an expansion velocity of 10 km s^{-1} (Bernat et al. 1979) and is detected in our C configuration image cube. Here, the CO

spectrum shows a blueshifted expansion velocity of 10 km s^{-1} in agreement with Bernat et al. (1979) and has a larger redshifted expansion velocity of 13 km s^{-1} . The extended CARMA C configuration is not sensitive to emission $\gtrsim 4.5''$ and provides little detail on the S2 velocity component which has an expansion velocity of 17 km s^{-1} (Bernat et al. 1979) and is known to be more extended than the S1 component (Bernat et al. 1979; Huggins 1986). An extreme blue wing of the CO spectrum appears in the D and E configuration image cubes at an expansion velocity of 16 km s^{-1} . These CARMA configurations are more sensitive to the extended S2 emission and as the expansion velocity of this blue wing is in close agreement with that reported by Bernat et al. (1979), we identify this extreme blue wing with the S2 velocity component. We do not detect a redshifted S2 velocity component in any of our spectra.

The spatial scales of the two shells (S1 and S2) have not been directly determined from either the CO infrared absorption spectra of Bernat et al. (1979) or previous single dish radio observations (Knapp et al. 1980; Huggins 1986; Huggins et al. 1994). Our combined configuration image cube has sufficient spatial resolution and signal-to-noise to make direct estimates for both shell sizes. The S1 shell extends out to an average distance of $\sim 4.5''$. It is more extended in the S-W direction due mainly to the presence of the second emission feature in the D configuration data. Our spatial resolution of $0.8''$ is not sufficient to determine whether the S1 shell is discrete. It is possible that this shell is an extension of the current wind phase seen in ultraviolet spectra (Carpenter et al. 1997) and cm-radio continuum interferometry (Lim et al. 1998; Harper et al. 2001) and we conclude that its inner radius is $< 0.8''$. The S2 shell extends out to a radius of at least $12''$ which is approximately the maximum distance we can sample out to with sufficient accuracy in the combined image. Our limited field of view means that we cannot conclude if the spatial scale of the S2 shell extends beyond $12''$.

The shape of our combined image cube spectra for circular extraction area with radii $6''$ or greater are in reasonable agreement with previous high signal to noise single dish CO(J=2-1) spectra. Our total line width of 29 km s^{-1} is in good agreement with Huggins (1986) and Huggins et al. (1994) who report line widths of 28.6 km s^{-1} and 30 km s^{-1} respectively. The blue wing in both of these spectra are the dominant emission features of the line and this is also true in our combined spectra at extraction areas $\gtrsim 6''$. The IRAM 30m telescope in Huggins et al. (1994) has a beam size of only $12''$ at 230 GHz and yet produces a similar line profile shape to Huggins (1986) who uses a larger beam size of $\sim 30''$. From this, one would expect that the majority of the blue wing emission is compact. However, our combined spectra show a continuous increase in the blue wing emission as we take larger extraction regions and as we can see a faint ring structure out to our field of view we believe the S2 shell is more extended than suggested by these previous single dish observations.

Support for CARMA construction was derived from the states of California, Illinois, and Maryland, the James S. McDonnell Foundation, the Gordon and Betty Moore Foundation, the Kenneth T. and Eileen L. Norris Foundation, the University of Chicago, the Associates of the California Institute of Technology, and the National Science Foundation. Ongoing CARMA development and operations are supported by the National Science Foundation under a cooperative agreement, and by the CARMA partner universities.

Facilities: CARMA

REFERENCES

- Bernat, A. P., Hall, N. B., Hinkle, K. H., & Ridgeway, S. T. 1979, ApJ, 233, L135
- Carpenter, K. G., & Robinson, R. D. 1997, ApJ, 479, 970
- Harper, G. M., Brown, A., & Lim, J. 2001, ApJ, 551, 1073
- Harper, G. M., Brown, A., & Guinan, E. F. 2008, AJ, 135, 1430
- Harper, G. M., Carpenter, K. G., Ryde, N., et al. 2009, AIP Conf. Ser., 1094, 868
- Huggins, P. J. 1986, ApJ, 313, 400
- Huggins, P. J., Bachiller, R., Cox, P., & Forveille, T. 1994, ApJ, 424, L127
- Knapp, G. R., Philips, T. G., & Huggins, P. J. 1980, ApJ, 242, L25
- Lim, J., Carilli, C., White, S. M., Beasley, A. J., Marson, R. G. 1998, Nature, 392, 575
- Rich, J. W., de Blok, W. J. G., Cornwell, T. J. et al. 2008, AJ, 136, 2897
- Scott, S. L., Amarnath, N.S., Kraybill, J. C. et al. 2004, in ASP Conf. Ser. 314, ADASS XIII, ed. F. Ochsenbein, M. Allen, D. Egret (San Francisco, CA: ASP), 768

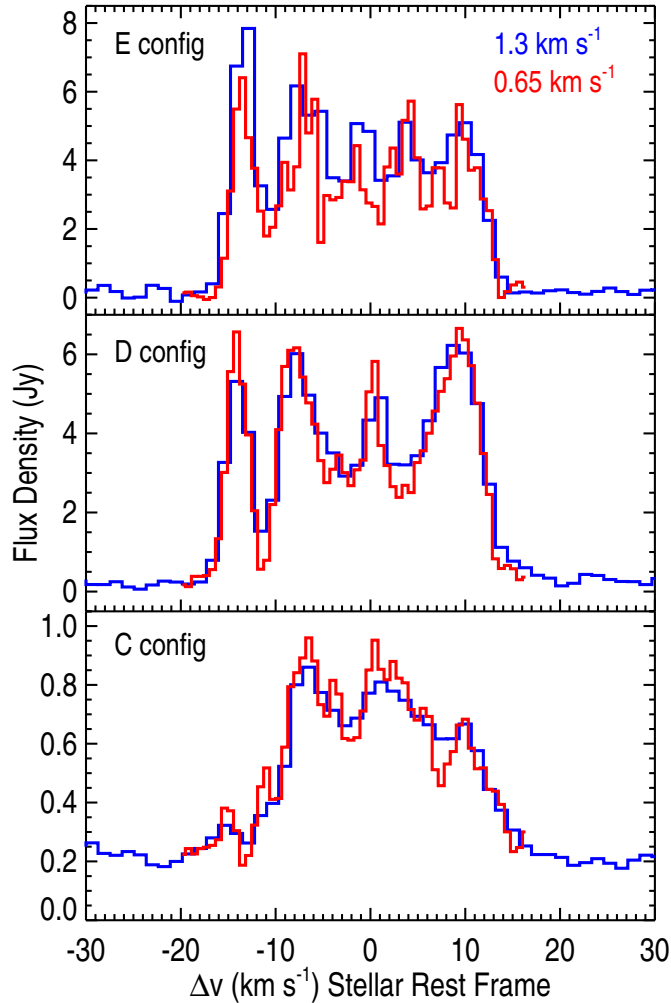


Fig. 1.— Spectra from the image cubes for each array configuration. The bottom panel shows the absence of the blueshifted emission component between -10 km s^{-1} and -16 km s^{-1} in the C configuration image cube spectrum.

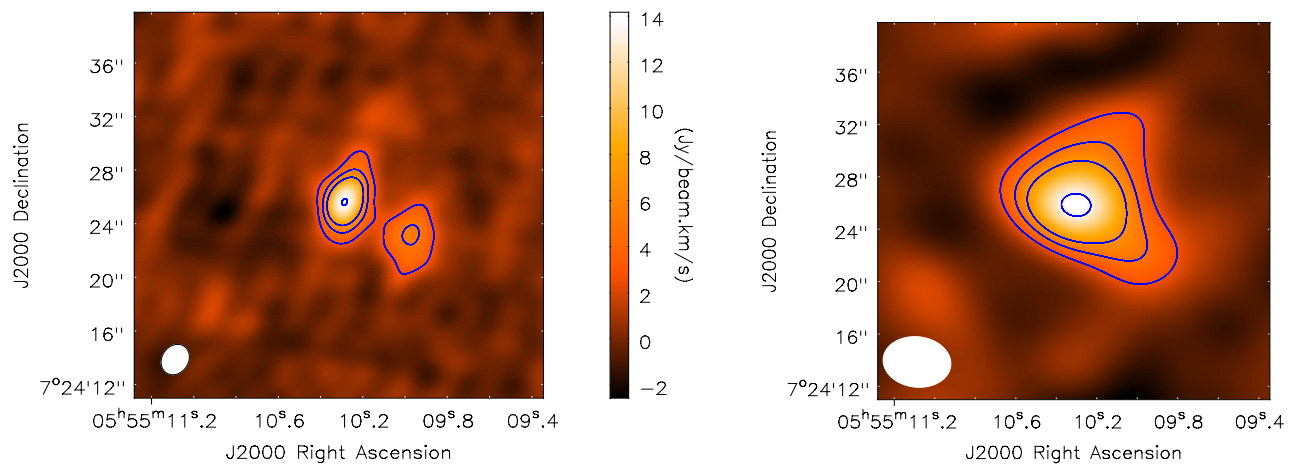


Fig. 2.— *Left:* Integrated intensity image of the D configuration channel maps that contain the discrete second source. Contours for the integrated intensity are 1σ , 1.5σ and 3σ ($1\sigma = 1.46 \text{ Jy beam}^{-1} \text{ km s}^{-1}$). *Right:* Integrated intensity image of the corresponding E configuration channel maps. Contours for the integrated intensity are again 1σ , 1.5σ and 3σ ($1\sigma = 2.94 \text{ Jy beam}^{-1} \text{ km s}^{-1}$). The size of the restoring beam is shown in white in the bottom left corner. Images have not been corrected for the primary beam response.

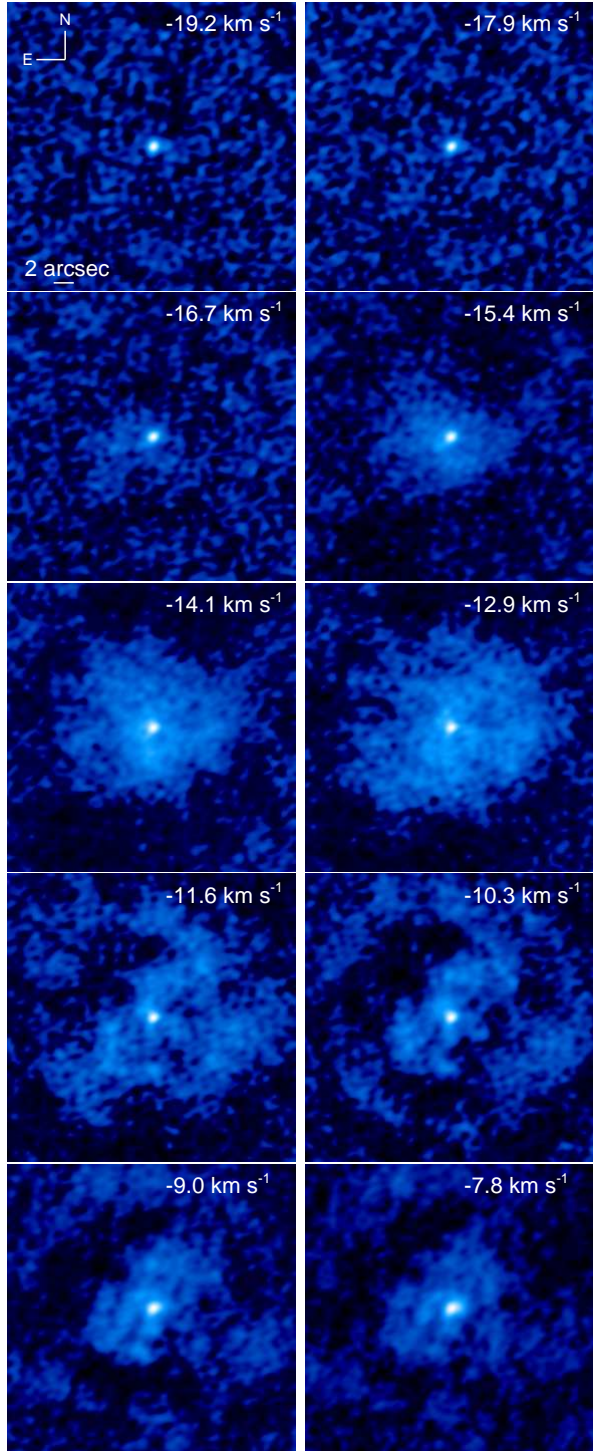


Fig. 3.— 10 channel maps from the combined configuration non-primary beam corrected image cube. The color scale has been normalized to the maximum and minimum value of each channel and is a function of the square root of the flux to emphasize the fainter emission.

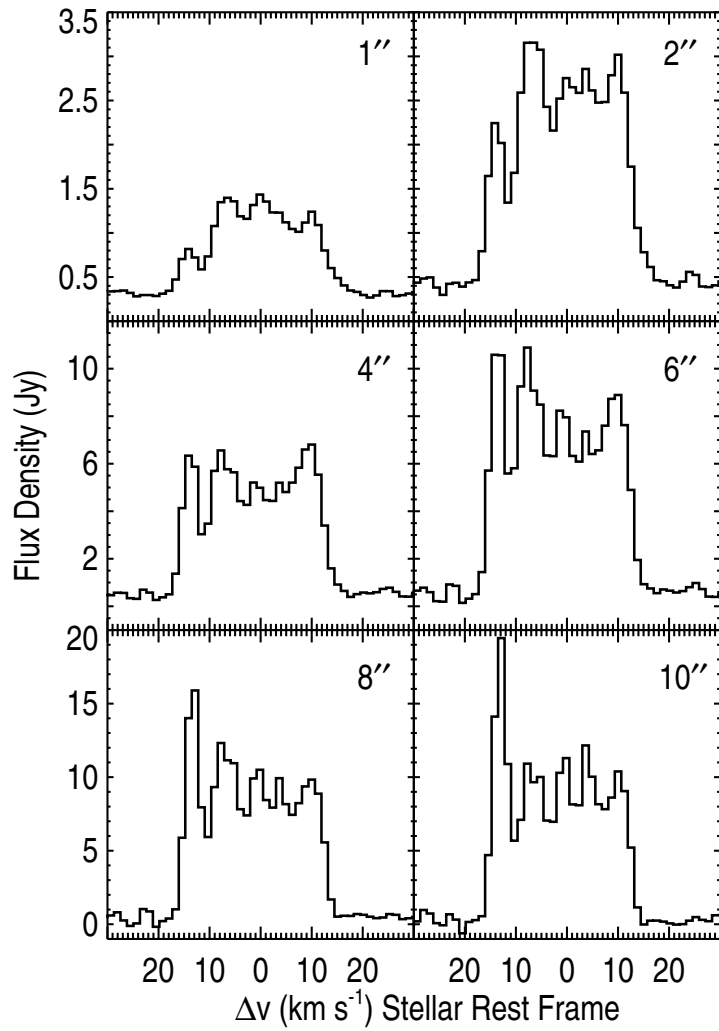


Fig. 4.— Spectral profiles of the combined image cube for circular extraction areas of radius 1'', 2'', 4'', 6'', 8'' and 10''.

Table 1. CARMA Observations

Observation Date	Configuration	Time on Source (hr)	Flux Calibrator	Phase Calibrators	Image Cube ^a Dynamic Range ^b
2007 May 11	D	1.2	0530+135	0530+135, 0532+075	11.00
2007 Jun 18	D	0.9	0530+135	0530+135, 0532+075	13.01
2007 Jun 21	D	3.0	0530+135	0530+135, 0532+075	12.98
2007 Jun 24	D	2.1	0530+135	0530+135, 0532+075	13.75
2007 Jun 25	D	2.4	0530+135	0530+135, 0532+075	15.66
2009 Jul 07	E	3.2	3C120	3C120, 0532+075	15.04
2009 Nov 05	C	1.2	3C120	3C120, 0532+075	10.94
2009 Nov 09	C	3.0	3C120	3C120, 0532+075	16.81
2009 Nov 15	C	1.0	3C120	3C120, 0532+075	11.35
2009 Nov 16	C	3.2	3C120	3C120, 0532+075	18.47
All	C	8.4	29.28
All	D	9.5	22.38
All	Combined	21.2	31.72

^aChannel width of 1.3 km s⁻¹ and not corrected for primary beam attenuation.^bThe peak emission of the image cube divided by the root mean square of the residual image.